ECCOMAS Congress 2016
VII European Congress on Computational Methods in Applied Sciences and Engineering
M. Papadrakakis, V. Papadopoulos, G. Stefanou, V. Plevris (eds.)
Crete Island, Greece, 5–10 June 2016

COMPARISON OF FINITE VOLUME HIGH-ORDER SCHEMES FOR THE TWO-DIMENSIONAL EULER EQUATIONS

Jens Wellner

German Aerospace Center (DLR),
Institute of Propulsion Technology,
Linder Höhe, 51147 Cologne, Germany
e-mail: Jens.Wellner@dlr.de

Keywords: High-order, Finite volume, Euler equations, MUSCL, WENO, compact scheme

Abstract. *The present paper describes the use of various high-order schemes in a finite volume formulation for use on structured grids. In particular, WENO and compact upwind schemes as well as central and upwind schemes are investigated. Their efficiency and accuracy are compared to the well-established second- and third-order MUSCL family of schemes. The different schemes are analyzed and tested numerically using canonical flow problems in the context of the two-dimensional Euler equations. Results are shown for the two-dimensional advection of a density pulse to quantify the dissipation and dispersion properties of the schemes. To investigate the non-oscillatory nature of the schemes and the resolution of discontinuities the Riemann problem is analyzed. The simulations are performed on uniform as well as non-uniform meshes.*

1 INTRODUCTION

Over the past decades there has much research into the design and application of high-order accurate numerical methods. In the context of computational fluid dynamics (CFD) high-order methods are especially desirable to simulate flows with complicated structures. In compressible flows, the existence of shocks, interfaces and other discontinuities present additional challenges to high-order schemes as, alongside providing high-order accuracy in smooth regions of the solution, they must remain non-oscillatory and stable in regions of high nonlinearity.

This paper examines the behavior of various high-order schemes in a finite volume formulation for the use of structured grids and compares their efficiency and accuracy to the well-established second- and third-order MUSCL family of schemes. In particular, weighted essentially non-oscillatory (WENO) and compact schemes show great potential for further improvements due to the fact that these schemes are active fields of research since many years. But also central and upwind schemes are good candidates for very efficient high-order schemes by the reason of their relatively simple nature.

The different schemes are analyzed and tested on both uniform and non-uniform grids in the context of the two-dimensional Euler equations. The accuracy, convergence and resolution are studied for the advection of a Gaussian entropy pulse and the non-oscillatory behavior across the discontinuities is investigated with the classical shock tube test problem by Sod [1].

2 THE FINITE VOLUME SCHEMES

2.1 Governing Equations

The flow of two-dimensional, compressible, inviscid fluid can be described in conservation form by the Euler equations:

$$\frac{\partial Q}{\partial t} + \frac{\partial F}{\partial x} + \frac{\partial G}{\partial y} = 0 \tag{1}$$

where $Q = (\rho, \rho u, \rho v, \rho e)^T$ and

$$F = \begin{pmatrix} \rho u \\ \rho u^2 + p \\ \rho uv \\ u\left(\rho e + p\right) \end{pmatrix}, \quad G = \begin{pmatrix} \rho v \\ \rho uv \\ \rho v^2 + p \\ v\left(\rho e + p\right) \end{pmatrix}.$$

Here p, ρ, u, v and e are the pressure, density, velocity components and the total energy per unit mass, respectively. The pressure is given by the equation of state for perfect gas:

$$p = \left(\gamma - 1\right)\rho\left(e - \frac{1}{2}\left(u^2 + v^2\right)\right)$$

where γ is the ratio of specific heats.

Considering a structured mesh, the finite volume formulation is derived by integrating Eq. 1 on an interval $\left[x_{i-1/2,j}, x_{i+1/2,j}\right] \times \left[y_{i,j-1/2}, y_{i,j+1/2}\right]$

$$\frac{\partial}{\partial t}\bar{Q}_{i,j} = -\frac{1}{\Delta_i x \Delta_j y}\left(F_{i+1/2,j} - F_{i-1/2,j} + G_{i,j+1/2} - G_{i,j-1/2}\right) \tag{2}$$

where

$$\bar{Q}_{i,j} = \frac{1}{\Delta_i x \Delta_j y}\int_{x_{i-1/2,j}}^{x_{i+1/2,j}}\int_{y_{i,j-1/2}}^{y_{i,j+1/2}} Q dx dy$$

is the cell average of $\bar{Q}$ in the (i,j)-th cell. The Gaussian quadrature used to integrate the flux on each cell interface is second-order accurate.

Temporal integration in Eq. 2 can be accomplished by treating this as a system of ordinary differential equations, via a method-of-lines approach. In particular, the explicit third-order Runge-Kutta method of Gottlieb and Shu [2] will be used. This method is high-order accurate and total-variation diminishing (TVD) in the sense that the temporal operator does not increase the solution's total variation in time.

$$\begin{aligned}\bar{Q}^{(1)} &= \bar{Q}^{(n)} + \Delta t \mathbf{R}(\bar{Q}^{(n)}) \\ \bar{Q}^{(2)} &= \frac{3}{4}\bar{Q}^{(n)} + \frac{1}{4}\bar{Q}^{(1)} + \frac{1}{4}\Delta t \mathbf{R}(\bar{Q}^{(1)}) \\ \bar{Q}^{(n+1)} &= \frac{1}{3}\bar{Q}^{(n)} + \frac{2}{3}\bar{Q}^{(2)} + \frac{2}{3}\Delta t \mathbf{R}(\bar{Q}^{(2)})\end{aligned}$$

Where $\mathbf{R}$ is the right hand side of Eq. 2.

The fluxes in $\mathbf{R}$ are approximated by solving the local Riemann problems at the cell interfaces with a solver due to Roe [3] for all asymmetric discretization schemes. E.g. for

$$F_{i+1/2,j} = \frac{1}{2}\left(F^L_{i+1/2,j} + F^R_{i+1/2,j}\right) - |A|\left(U^L_{i+1/2,j} + U^R_{i+1/2,j}\right)$$

where A is the Roe matrix with $U = (\rho, u, v, p)^T$. In the case of symmetric schemes, for which U^L and U^R are identical the fluxes are directly evaluated from the flow state at the cell interface position.

2.2 Discretization Schemes

To obtain the face fluxes the left and right states of U are computed. There are several choices of the variable to be reconstructed, such as the primitive, conservative or characteristic variables. In the context of this paper for all investigated schemes the primitive variables are used even if it is recommended to use the characteristic variables in context of WENO schemes for shock simulation (see e.g. Borges et al. [4]). The reconstruction with all investigated schemes are accomplished in a dimension-by-dimension fashion. For the sake of brevity only the reconstruction of the left state is denoted here.

The first class of discretization schemes are the well-established second- and third-order MUSCL (Monotonic Upstream-Centered Scheme for Conservation Laws) family.

$$U^L_{i+1/2} = \bar{U}_i + \frac{1}{4}\left[(1+\kappa)\, r_i \Phi\left(1/r_i\right) + (1-\kappa)\,\Phi\left(r_i\right)\right]\left(\bar{U}_i - \bar{U}_{i-1}\right) \tag{3}$$

The function $\Phi\left(r_i\right)$ is a limiter function to limit the slopes r_i. The parameter k determines the spatial accuracy of the interpolation. In this work the minmod, Van Leer, superbee, monotonized central, Van Albada and Van Albada 2 limiter functions are considered for uniform meshes. Zeng [5] proposed also non-uniform versions of the limiter functions for minmod, Van Leer, superbee, monotonized central and Van Albada. Leng et al. [6] developed an optimized MUSCL scheme to minimize the dissipation and dispersion error in combination with the monotonized central limiter. This family of schemes is usually second or third-order, since it is difficult to develop limiter functions for higher-order MUSCL schemes.

The second class of discretization schemes are the WENO (weighted essentially non-oscillatory) schemes.

$$U^L_{i+1/2} = \sum_{k=0}^{r-1} \omega_k q^r_k \tag{4}$$

q_k^r are rth-order accurate polynomial interpolants evaluated at $x_{i+1/2}$ computed by

$$q_k^r = \sum_{l=0}^{r-1} a_{kl}^r \bar{U}_{i-r+k+l+1}$$

where a_{kl}^r are stencil coefficients. The weights are defined by

$$\omega_k = \frac{\alpha_k}{\sum_{k=1}^{r-1} \alpha_k} \tag{5}$$

and

$$\alpha_k = \frac{C_k^r}{(\epsilon + \beta_k)^2}.$$

where

$$\beta_k = \sum_{m=1}^{r-1} \left(\sum_{l=1}^{r-1} d_{kml}^r \bar{U}_{i-r+k+l+1} \right)^2$$

and ϵ is small number designed to prevent division by zero. The smoothness indicators β_k become large when discontinuities are present within the stencil k and remain relatively small otherwise.

In the case of odd-order WENO schemes considered here an one point upwind biased interpolation polynomials are used for q_k^r. For the classical fifth-order WENO scheme after Jiang and Shu [7] the above definition results in a convex combination of three third-order candidate stencils. This version is denoted as WENOJS in the rest of the paper. In critical points where multiple derivatives vanish the weight ω_k are far away from the optimal weights C_k^r and the order of convergence decreases dramatically. In the literature several approaches have been proposed to recover the formal order of accuracy in the smooth regions of the solution. In this work, in addition to the above formulation in Eq. 5, the modified weighting procedures WENOM after Hendricks et al. [8], WENOZ after Borges et al. [4], WENOYC after Yamaleev and Carpenter [9], WENOZS after Shen and Zha [10] and WENON after Xiaoshuai and Yuxin [11] are considered. Within the context of WENO schemes the sensitivity parameter ϵ is also a subject of active research and can cause a drop of the rate of convergence in some cases. In this work both constant values ranging between 10^{-60} and 10^{-2} are used as well as methods suggested by Peer et al. [12], Yamaleev and Carpenter [9] and Don and Borges [13].

Martin et al. [14] developed a central symmetric WENO scheme. Since in classical WENO schemes the center of the stencil collection lies slightly upwind of the reconstruction point the WENO scheme proposed by Martin et al. uses an additional stencil to form a symmetric central scheme which is capable of providing zero dissipation.

Additional class of schemes investigated are compact schemes. The general form of the interpolation formula for the cell faces is

$$\alpha U_{i-1/2}^L + U_{i+1/2}^L + \beta U_{i+3/2}^L = a\bar{U}_{i-2} + b\bar{U}_{i-1} + c\bar{U}_i + d\bar{U}_{i+1}. \tag{6}$$

Here only compact upwind interpolations with narrow stencils are considered so as to use efficient matrix inversion algorithms of a tridiagonal matrix, such as the Thomas algorithm. The used coefficients of Eq. 6 can be found in Tab. 1. For a more detailed description of the schemes see Broeckhoven et al. [15]. Following the notation of Broeckhoven et al. two different types of upwind-biased interpolations are investigated. The implicit (left-hand side) part purely central and the explicit (right-hand side) part upwind-biased (ICxEUyz). Here x is the number of

Scheme	Order	α	β	a	b	c	d
IC3EU22	3	$-\frac{1}{5}$	$-\frac{1}{5}$	0	$-\frac{3}{10}$	$\frac{9}{10}$	0
IC3EU33	4	$-\frac{1}{8}$	$-\frac{1}{8}$	$\frac{1}{8}$	$-\frac{5}{8}$	$\frac{5}{4}$	0
IC3EU43	5	$-\frac{3}{14}$	$-\frac{3}{14}$	$\frac{1}{84}$	$-\frac{5}{84}$	$\frac{67}{84}$	$\frac{19}{28}$
IU22EU21	3	$\frac{1}{2}$	0	0	0	$\frac{5}{4}$	$\frac{1}{4}$
IU32EU32	5	$\frac{1}{2}$	$\frac{1}{6}$	0	$\frac{1}{18}$	$\frac{19}{18}$	$\frac{5}{9}$

Table 1: Overview of different coefficients of compact schemes

points in the implicit and y the number of points in the explicit part. z indicates the position of $\bar{U}_i$. And both implicit and explicit part upwind-biased (IUxyEUzw). Here x is the number of points in the implicit and z the number of points in the explicit part. y indicates the position of $U_{i+1/2}$ and w indicates the position of $\bar{U}_i$. For periodic problems these schemes are solved using the Thomas Algorithm for periodic tridiagonal systems. Otherwise the standard Thomas Algorithm is used by applying different boundary closures to IU32EU32 (compactBC), which can be found in Pirozzoli [16] and Ghosh and Baeder [17]. Also the impact to the accuracy and stability of the application of an explicit central filter is investigated to reduce non-physical oscillations.

The last class of schemes are simple explicit upwinding (Eq. 7), symmetric (Eq. 8) and asymmetric (Eq. 9) central schemes without any stabilization techniques such as limiters or filtering. These schemes are based upon Lagrange interpolation polynomials which are also used to construct the WENO schemes. Therefore, they can be considered as WENO schemes with fixed optimal weights C_k^r.

$$U^L_{i+1/2} = a\bar{U}_{i-3} + b\bar{U}_{i-2} + c\bar{U}_{i-1} + d\bar{U}_i + e\bar{U}_{i+1} + f\bar{U}_{i+2} + g\bar{U}_{i+3} \tag{7}$$

$$U^{L,R}_{i+1/2} = a\bar{U}_{i-3} + b\bar{U}_{i-2} + c\bar{U}_{i-1} + d\bar{U}_i + d\bar{U}_{i+1} + c\bar{U}_{i+2} + b\bar{U}_{i+3} + a\bar{U}_{i+4} \tag{8}$$

$$U^L_{i+1/2} = a\bar{U}_{i-3} + b\bar{U}_{i-2} + c\bar{U}_{i-1} + d\bar{U}_i + e\bar{U}_{i+1} + f\bar{U}_{i+2} + g\bar{U}_{i+3} + h\bar{U}_{i+4} \tag{9}$$

Tab. 2 provides an overview of the reviewed methods, their order of accuracy and used acronym for the rest of this paper. The theoretical order of convergence is denoted with a number after the scheme acronym if appropriate.

3 NUMERICAL RESULTS

The application of the described schemes to the two-dimensional Euler equations is discussed in this section. The accuracy and convergence properties are studied on a smooth problem that involves the advection of a Gaussian entropy pulse. The non-oscillatory nature of the schemes and the resolution of discontinuities are studied in this section using the Riemann problem.

3.1 Entropy Advection

The advection of a smooth density pulse over a periodic domain is considered in this section. The pressure and velocity fields are constant, thus reducing the Euler equations to a linear advection equation for density, with the advection speed as the freestream velocity. The exact

Scheme	Acronym	Implemented Order	Equation
Monotonic Upstream-Centered Scheme for Conservation Laws	MUSCL	1, 2, 3	3
Optimized MUSCL	oMUSCL	2	-
MUSCL for non-uniform grids	nuMUSCL	2	-
Weighted Essentially Non-oscillatory Schemes	WENO	3, 5, 7	4
Central symmetric WENO	CWENOSym	4, 6, 8	-
Compact upwind scheme	compact	3, 4, 5	6
one point upwind biased scheme	upwind	3, 5, 7	7
central symmetric schemes	centralSym	2, 4, 6, 8	8
centralSym for non-uniform grids	nuCentralSym	2, 4, 6, 8	8
central asymmetric schemes	centralASym	2, 4, 6, 8	9
optimized centralASym	oCentralSym	5, 7	9

Table 2: Overview of review discretization schemes

solution is given by:

$$\begin{aligned}
\rho\left(x,y,t\right) &= \rho_\infty + Ae^{-\left((x-u_\infty t)^2+y^2\right)} \\
u\left(x,y,t\right) &= u_\infty \\
v\left(x,y,t\right) &= v_\infty \\
p\left(x,y,t\right) &= p_\infty
\end{aligned}$$

In the present example, the freestream conditions are taken as $\rho_\infty = 1.2\,\mathrm{kg/m^3}$, $u_\infty = 180\,\mathrm{m/s}$, $v_\infty = 0\,\mathrm{m/s}$, $p_\infty = 94040\,\mathrm{Pa}$ and the amplitude of the entropy wave is taken as $A = 0.05\,\mathrm{kg/m^3}$. The domain is taken as $[-25\,\mathrm{m}, 25\,\mathrm{m}] \times [-25\,\mathrm{m}, 25\,\mathrm{m}]$ and periodic boundaries are assumed on both sides. The solution is obtained after one cycle ($t = L/u_\infty = 0.28\,\mathrm{s}$) and the L_1 error norms are compared. An initial grid with 21 points is taken and progressively refined. The CFL number corresponding to the grid with 21 points is 0.08 and is decreased with each grid refinement, to ensure that errors due to time discretization converge at the same order as those due to space discretization.

The simulations were carried out on three different grids, see Fig. 1. This first consists of uniform distributed cells. The second is a non-uniform grid where every i constant line (and every j constant line) has been shifted in the x-direction (or respectively the y-direction) by a random distance. The last investigated grid is additionally distorted by a random shift of every vertex and every second i constant line shifted in y-direction by a constant distance.

Fig 2 shows the convergence rate of the various scheme classes on the uniform grid. The L_1 errors from the simulations with different formulation in one class of schemes are averaged. This way it is possible to compare not only single schemes with each other but rather to get an overview of the different classes. With every grid refinement the error decreases. But since every scheme shows the theoretical order of convergence for this simple test case a clustering of schemes can be observed.

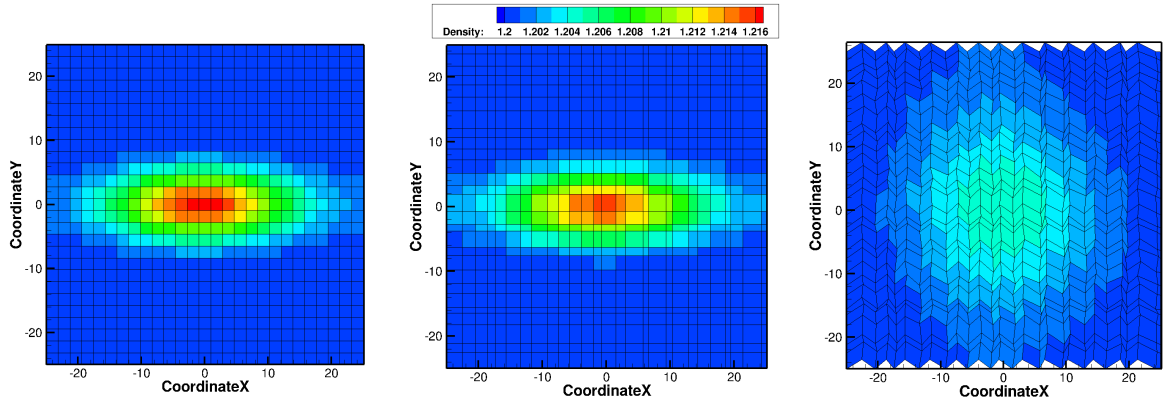

(a) uniform grid (b) non-uniform grid (c) distorted grid

Figure 1: Solution of the advection of a density pulse with MUSCL1

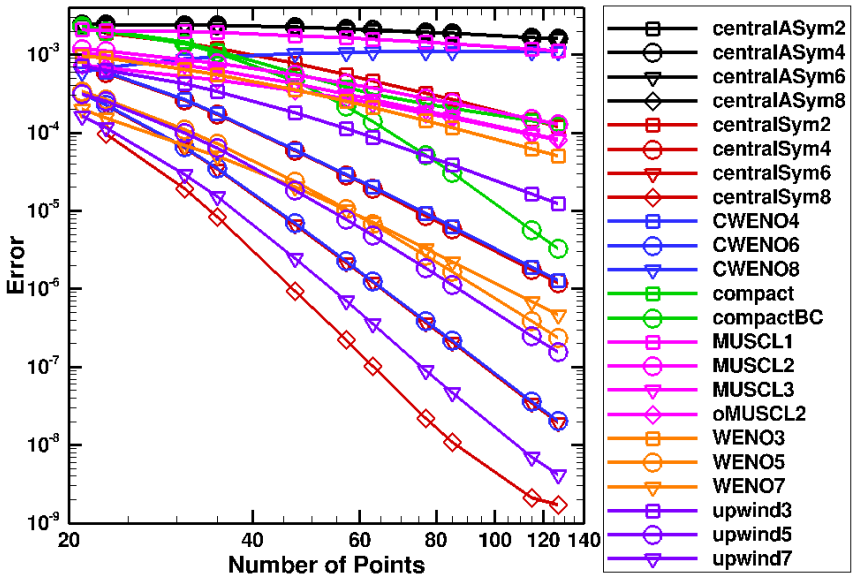

Figure 2: Convergence rate of various scheme classes for the advection of a density pulse on uniform grids

In order to choose an efficient scheme, it is helpful to consider the simulation duration instead of the number of cells for a given accuracy. In Fig. 3 error versus the wall-clock time required to obtain the solution on the given grid. Each symbol represents one grid tested with all schemes. Here it is easy to see that the simple schemes use significant less computational effort to reach a certain level of error. E.g. the advantage of the upwind5 compared to the WENO5 scheme is evident in Fig. 3(a) but not in Fig. 2. Since the upwind and central schemes are constructed without any shock-capturing abilities, they offer a very efficient possibility to simulate wave propagation phenomenon in smooth flow regimes. Also the high-order versions are preferable due to lower dissipation. In the category of shock-capturing schemes, in the direct comparison of MUSCL3 and WENO3, it appears that the computational cost to determine the non-linear weights in the WENO schemes can not be compensated by a lower error. Especially the oMUSCL2 scheme shows advantages on coarse grids. Due to the wave number optimization they are able to provide lower dissipation on these grids. The compact schemes are not able to show the ability to provide a high spectral resolution. Here spurious oscillations appear even with the use of upwind biased compact schemes which contaminate the solution. To address this problem an explicit central filter (see [18]) was used but it was found to reduce the accuracy. Still compact schemes including an inversion of a tridiagonal matrix seems to be faster than WENO schemes. For the class of central schemes shown in Fig. 3(b) there is a similar pattern. The centralSym schemes are very efficient since there is no need to solve a Riemann problem at the cell interfaces. So the computational effort is smaller than for any upwind biased scheme. However, their use is limited to only a few very simple flow conditions. CWENO schemes have also no need for a Riemann solver but the computation of the expensive non-linear weights is needed. The high error in the solutions with the centralASym is due to the fact than the advection speed is overestimated.

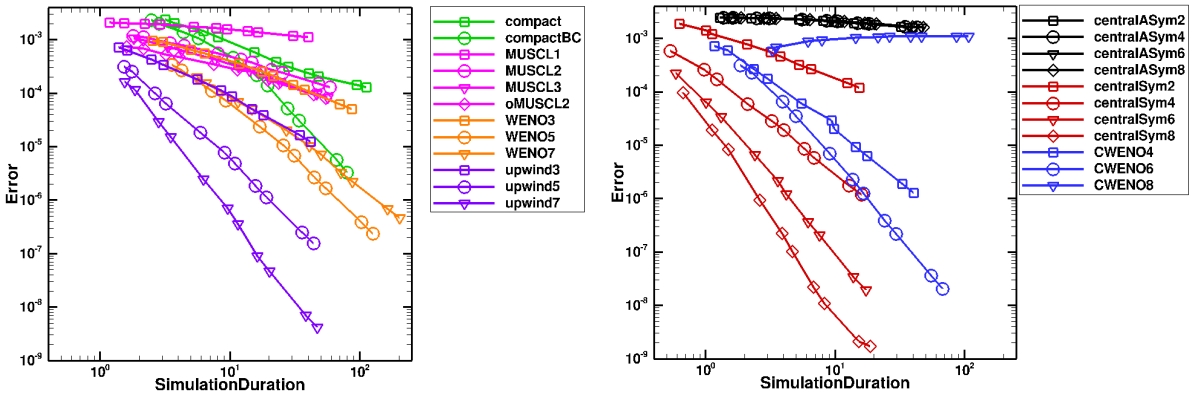

(a) upwind biased schemes (b) central schemes

Figure 3: Efficiency of various scheme classes for the advection of a density pulse on uniform grids

On non-uniform grids all schemes investigated produce significantly higher errors and even the rate convergence drops to mainly second-order. Furthermore, it is found that the upwind schemes designed for uniform grids produce the lowest error. Only the non-uniform formulation of the MUSCL2 schemes can give comparable results. Most notably the compact schemes are very sensitive to non-uniform spacing and have only first-order accuracy. However, most central schemes were not able to provide acceptable solutions due to the high stretching ratios in the grid. For the third grid type, the distorted grid, the situation is even worse. No scheme class is able to achieve a first-order convergence rate. Actually the nuMUSCL2 have a convergence

rate of 0.48. This scheme is designed to take a stretching ratio into account, but still relies on cell orthogonal to the flow direction.

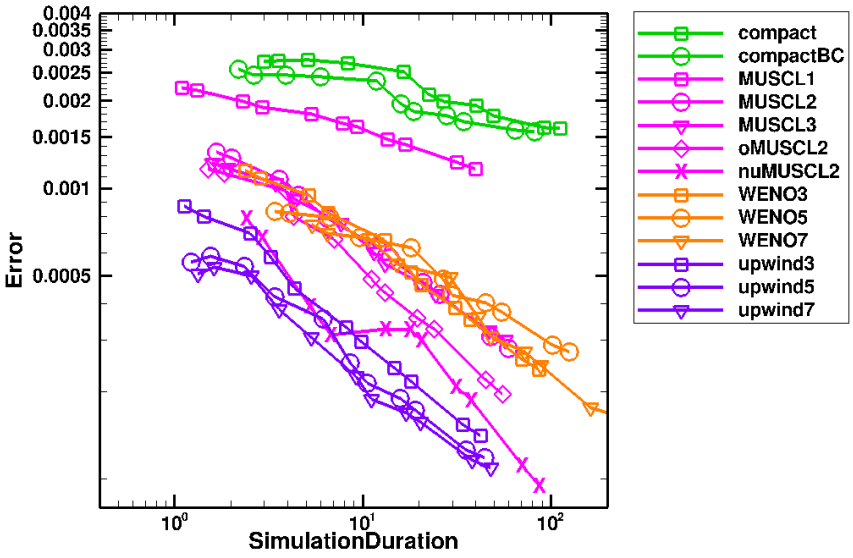

Figure 4: Efficiency of upwind biased schemes for the advection of a density pulse on non-uniform grids

3.2 Sod Shock Tube Problem

The non-oscillatory nature of the schemes and the resolution of discontinuities are assessed using a Riemann problem. The problem consists of an initial discontinuity that decomposes into a rarefaction wave, a contact discontinuity and a shock wave, corresponding to each of the characteristic fields of the Euler equations. The Sod shock tube problem [1] is an inviscid benchmark problem. The exact solution to this problem is obtained using a Riemann solver. The initial conditions are:

$$\rho_L = 1\,\mathrm{kg/m^3},\ u_L = 0\,\mathrm{m/s},\ v_L = 0\,\mathrm{m/s},\ p_L = 100000\,\mathrm{m/s}$$
$$\rho_R = 0.125\,\mathrm{kg/m^3},\ u_R = 0\,\mathrm{m/s},\ v_R = 0\,\mathrm{m/s},\ p_R = 10000\,\mathrm{m/s}$$

The domain is taken as $[-10\,\mathrm{m}, 10\,\mathrm{m}] \times [-10\,\mathrm{m}, 10\,\mathrm{m}]$ and the initial discontinuity is placed at $x = 0\mathrm{m}$. The solution is obtained at $t = 0.01\,\mathrm{s}$ on a grid with 20 points, a CFL number of 0.1 and is decreased with each grid refinement.

The analytical solution for the density and pressure at $y = 0\mathrm{m}$ is shown in Fig. 5. In addition, the simulation results obtained on an uniform grid with the first-order MUSCL scheme, the most efficient schemes of the MUSCL and WENO classes and upwind scheme are presented. Due to the relatively high dissipation of the MUSCL1 scheme the discontinuity is smeared while the Upwind5 scheme shows strong oscillations. The MUSCL2 scheme with the superbee limiter and WENOYC3 are able to sharply resolve the contact discontinuity and the shock wave.

An overview of the efficiency averaged for the different classes can found in Fig. 6. The results for compact schemes are not shown since it was not possible to obtain stable solutions for this test case. The other central schemes as expected suffer from severe oscillations and are not able to produce comparable smooth solutions. The WENO and upwind (a.k.a. optimal WENO) classes show a similar efficiency behavior. The calculation of the non-linear weights in the WENO schemes produces a large computational overhead that is not compensated by the

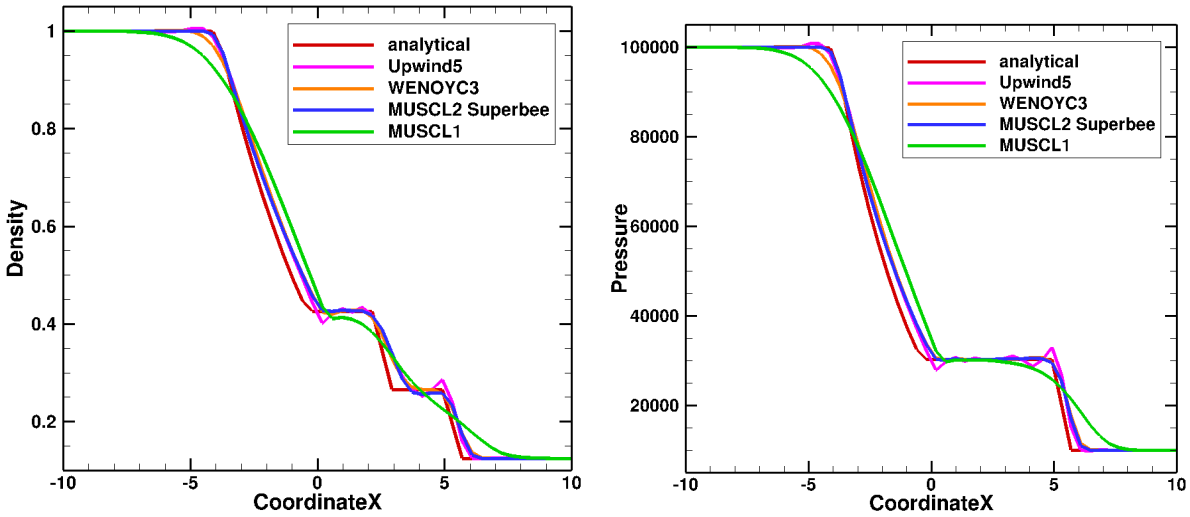

(a) Density (b) Pressure

Figure 5: Solution of Sod shock tube problem with exemplary schemes

higher accuracy. However, this observation does no longer hold for stronger shocks since the stencil of the simple upwind schemes uses cells containing the shock and becomes unstable. Through the construction of WENO schemes the use of these cells is reduced. The candidate stencils which contain the discontinuities are assigned a nearly zero weight in the formation of the final interpolation polynomial. The well-established MUSCL scheme class is able to create fast a solution with only minimal oscillations at a low level of errors.

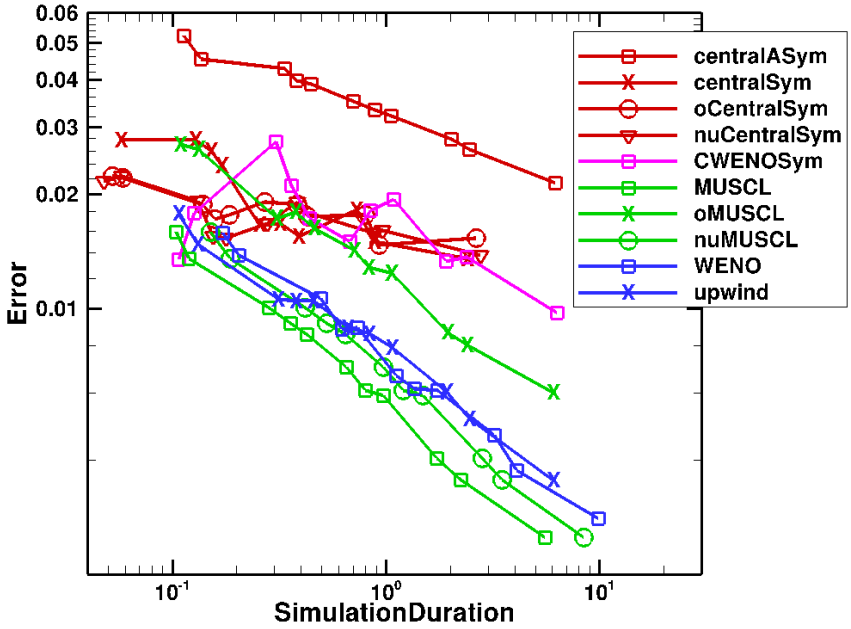

Figure 6: Efficiency for the Sod shock tube problem

To have a more detailed look only the best versions of each upwind biased class is shown in Fig. 7. For the MUSCL class the second-order schemes seem to represent the best choice. Within the context of the WENO schemes only the seventh-order method is not able the compensate the computational overhead with a lower error. Note, even the most efficient versions

of these shock-capturing schemes need significantly more computational time than the upwind schemes. Since this test case simulates a moderate shock problem the oscillations are not critical for the stability of the simulation. But in the presence of stronger shocks the MUSCL2 and WENO5 versions show better results. The non-uniform version of the MUSCL family is also

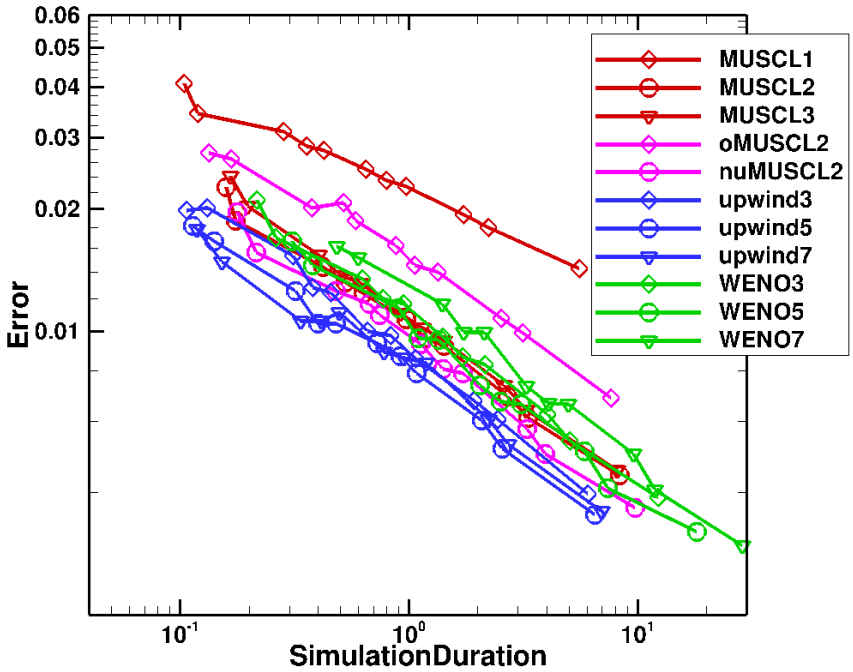

Figure 7: Efficiency of best versions of upwind biased scheme classes

able to reach the same accuracy, but is slightly more expensive. When applied to non-uniform grids, however these methods are found to be more efficient than their uniform counterparts as non-uniform parameter provides greater accuracy.

Of particular interest for the accuracy of WENO schemes especially near critical points, is the formulation of the non-linear weights. In Fig. 8 the analysis of all used accuracy order and sensitivity parameter formulations illustrated. Here the average of all WENO schemes, alongside the method with the best and worst efficiency is shown. The WENOM formulation has a significant larger computational cost. The other versions lie close together while the WENOYC seems to be the best choice within the WENO family.

In Tab. 3 the convergence order of the analyzed sets of schemes is documented. No class is able to provide a first-order convergence for the L_1-error even on uniform grids. The WENO schemes have a slightly better convergence rate than the MUSCL schemes. However, in terms of efficiency they are not able to outperform the MUSCL schemes due to the expensive calculation of the non-linear weights. In general, in the case of stronger shocks or non-uniform or distorted grids the total error increases and the order of convergence drops. Although the effect is only marginal this holds also for non-uniform schemes.

4 CONCLUSIONS

In this paper, the well-established MUSCL family of schemes are compared to modern shock-capturing WENO schemes, compact schemes of high-order accuracy and simple upwind and central schemes. Numerical experiments were performed by means of academic test cases within the framework of the two-dimensional Euler equations on uniform and non-uniform

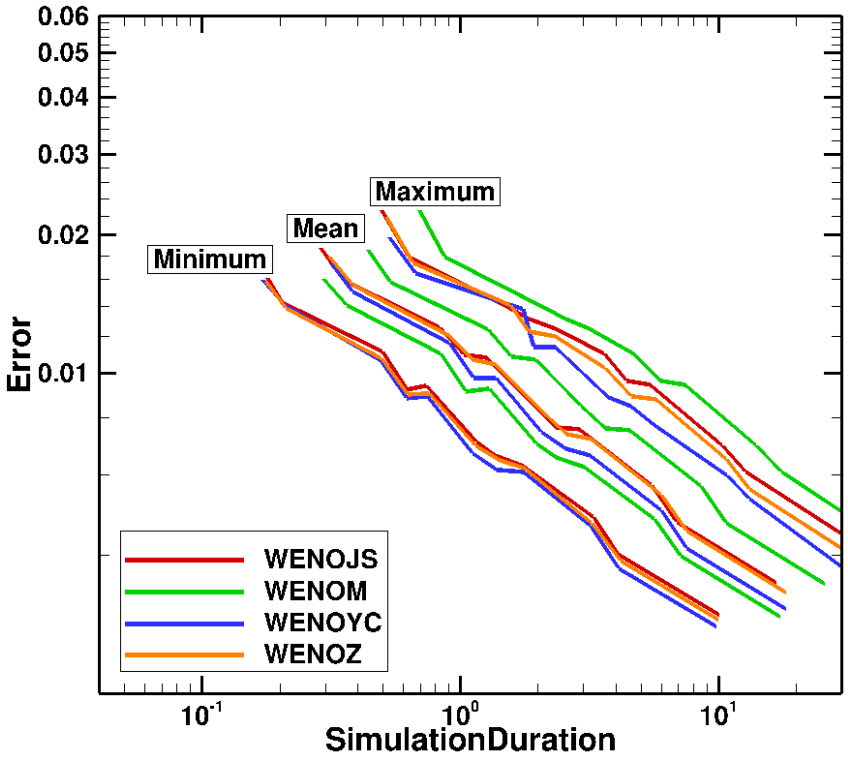

Figure 8: Efficiency distribution of WENO weight formulations

Scheme class		Convergence Order	
		uniform grid	non-uniform grid
MUSCL		0.83	0.70
	MUSCL1	0.54	0.52
	MUSCL2	0.86	0.73
	MUSCL3	0.89	0.72
	oMUSCL2	0.69	0.41
	nuMUSCL2	0.89	0.81
WENO		0.87	0.78
	WENOJS	0.87	0.75
	WENOM	0.86	0.66
	WENOYC	0.90	0.83
	WENOZ	0.87	0.77
upwind		0.80	0.77
centralASym		0.47	0.40
centralSym		0.45	0.34

Table 3: Order of convergence for Sod shock tube problem on uniform grids for different scheme classes

grids. It is found, for a given computational effort, that the high-order schemes are better able to accurately propagate wave disturbances. In particular, the simple upwind and central schemes show high efficiency in smooth flow regimes on uniform grids. On non-uniform grids, however, the order of accuracy drops for all investigated schemes and the absolute error level increases. Here the extra computational cost for non-uniform coefficients is found to be justified. In the case of discontinuities, the shock-capturing schemes are found to be superior over the simple schemes, since these schemes are not able to obtain an oscillation free stable solution. In terms of efficiency the MUSCL family provides good results. The WENO schemes show comparable results, but are not able to outperform the MUSCL schemes due to the high computational cost of the non-linear weights.

ACKNOWLEDGMENTS

The author would like to thank the Numerical Methods department at the Institute of Propulsion Technology at DLR and in particular Graham Ashcroft for his advice and many helpful discussions on this research.

REFERENCES

[1] Gary A. Sod. A survey of finite difference methods for systems of nonlinear hyperbolic conservation laws. *J. Comput. Phys.*, 27:1 – 31, 1978.

[2] Sigal Gottlieb and Chi-Wang Shu. Total variation diminishing Runge-Kutta schemes. *Mathematics of computation*, 67(211):73 – 85, January 1998.

[3] P. L. Roe. Approximate Riemann solvers, parameter vectors, and difference schemes. *Journal of Computational Physics*, 43(2):357–372, 1981.

[4] Rafael Borges, Monique Carmona, Bruno Costa, and Wai Sun Don. An improved weighted essentially non-oscillatory scheme for hyperbolic conservation laws. *Journal of Computational Physics*, 227(6):3191 – 3211, 2008.

[5] Xianyi Zeng. A general approach to enhance slope limiters on non-uniform grids. *SIAM J. Sci. Comput.*, January 2013.

[6] Yan Leng, XinLiang Li, DeXun Fu, and YanWen Ma. Optimization of the MUSCL scheme by dispersion and dissipation. *Science China Physics, Mechanics and Astronomy*, 55(5):844 – 853, 2012.

[7] Guang-Shan Jiang and Chi-Wang Shu. Efficient implementation of weighted ENO schemes. *J. Comput. Phys.*, 126(1):202 – 228, June 1996.

[8] Andrew K. Henrick, Tariq D. Aslam, and Joseph M. Powers. Mapped weighted essentially non-oscillatory schemes: Achieving optimal order near critical points. *J. Comput. Phys.*, 207(207):542 – 567, March 2005.

[9] Nail K. Yamaleev and Mark H. Carpenter. Third-order energy stable WENO scheme. *J. Comput. Phys.*, 228(8):3025 – 3047, 2009.

[10] Yiqing Shen and Gecheng Zha. Improvement of weighted essentially non-oscillatory schemes near discontinuities. *Computers & Fluids*, 96:1 – 9, February 2014.

[11] Wu Xiaoshuai and Zhao Yuxin. A high-resolution hybrid scheme for hyperbolic conservation laws. *Int. J. Numer. Meth. Fl.*, 78(3):162 – 187, 2015.

[12] A.A.I. Peer, M.Z. Dauhoo, and M. Bhuruth. A method for improving the performance of the WENO5 scheme near discontinuities. *Applied Mathematics Letters*, 22(11):1730 – 1733, 2009.

[13] Wai-Sun Don and Rafael Borges. Accuracy of the weighted essentially non-oscillatory conservative finite difference schemes. *J. Comput. Phys.*, 250:347 – 372, October 2013.

[14] M. P. Martin, E. M. Taylor, M. Wu, and V. G. Weirs. A bandwidth-optimized WENO scheme for the effective direct numerical simulation of compressible turbulence. *J. Comput. Phys.*, 220(1):270 – 289, December 2006.

[15] Tim Broeckhoven, Sergey Smirnov, Jan Ramboer, and Chris Lacor. Finite volume formulation of compact upwind and central schemes with artificial selective damping. *J. Sci. Comput.*, 21(3):341 – 367, December 2004.

[16] Sergio Pirozzoli. Conservative hybrid compact-WENO schemes for shock-turbulence interaction. *J. Comput. Phys.*, 178(1):81 – 117, May 2002.

[17] Debojyoti Ghosh and James D. Baeder. Compact Reconstruction Schemes with Weighted ENO Limiting for Hyperbolic Conservation Laws. *SIAM J. Sci. Comput.*, 34(3):A1678 – A1706, January 2012.

[18] Mei Zhuang and Christoph Richter. Computational aeroacoustics and its applications, 2007. Notes of the lecture series Computational Aeroacoustics at the Technical University Berlin.